

DMD 7153

STRUCTURAL ELUCIDATION OF HUMAN OXIDATIVE METABOLITES OF MURAGLITAZAR: USE OF MICROBIAL BIOREACTORS IN THE BIOSYNTHESIS OF METABOLITE STANDARDS

DONGLU ZHANG, HAIYING ZHANG, NELLY ARANIBAR, RONALD HANSON,
YANDE HUANG, PETER T CHENG, SHUNG WU, SAMUEL BONACORSI,
MINGSHE ZHU, ARUN SWAMINATHAN, AND W GRIFFITH HUMPHREYS

Pharmaceutical Candidate Optimization (DZ, HZ, NA, MZ, WH), Process
Development (RH), Analytical A&D (YH), Discovery Chemistry (PTC, SB, SW),
Clinical Discovery (AS), Pharmaceutical Research Institute, Bristol-Myers
Squibb, Princeton, NJ08543

DMD 7153

Running title: Human oxidative muraglitazar metabolites produced by microbial bioreactors

Address correspondence to:

Dr. Donglu Zhang,

Pharmaceutical Candidate Optimization,

Bristol-Myers Squibb, P.O. BOX 4000,

Princeton, NJ 08543.

Phone: 609-252-5582.

Email: Donglu.Zhang@BMS.com

¹Abbreviations used: HPLC, high performance liquid chromatography; LC/MS, liquid chromatography/mass spectrometry; NMR, nuclear magnetic resonance; CYP, cytochrome P450; PPAR, peroxisome proliferator-activated receptors; TFA, trifluoroacetic acid

Text pages (including references): 32

of tables: 3; # of figures: 8

of references: 23

of words in abstract: 245

of words in introduction: 350

of words in discussion: 850

ABSTRACT

Muraglitazar (Pargluva), a dual alpha/gamma PPAR activator, is currently in clinical development for treatment of type 2 diabetes. This study describes the structural elucidation of the human oxidative metabolites of muraglitazar through the use of a combination of microbial bioreactors, NMR and accurate mass analyses, and organic synthesis. Plasma, urine, and feces were collected from six healthy subjects following oral administration of C-14 labeled muraglitazar (10 mg, 100 microCi) and pooled samples were analyzed. Approximately 96% of the recovered radioactive dose was found in the feces and 3.5% in the urine. The parent compound represented >85% of the radioactivity in plasma. The fecal radioactivity was distributed among sixteen metabolites (M1-M12, M14-M16, and M8a) and the parent drug, of which hydroxylation and O-demethylation metabolites (M5, M10, M11, M14, and M15) represented the prominent human metabolites. The urinary radioactivity was distributed into several peaks including muraglitazar glucuronide (M13) and the parent drug. Low concentrations of metabolites in human samples prevented direct identification of metabolites beyond LC/MS analysis. Microbial strains *Cunninghamella elegans* and *Saccharopolyspora hirsuta* produced muraglitazar metabolites that had the same HPLC retention times and the same MS/MS properties as the corresponding human metabolites. The microbial metabolites M9, M10, M11, M14, M15, and M16 were isolated and analyzed by NMR. Based on these LC/MS/MS and NMR analyses, and organic synthesis, the structures of sixteen human oxidative metabolites were identified. The oxidative metabolism of muraglitazar was characterized by hydroxylation, O-demethylation, oxazole-ring opening, and O-demethylation /hydroxylation as well as O-dealkylation and carboxylic acid formation. This study demonstrated the utility of microbial bioreactors for the identification of metabolites.

INTRODUCTION

Peroxisome proliferator-activated receptors (PPARs)¹ are a set of nuclear hormone receptors (comprising the α , γ and δ subtypes). The two most intensively investigated subtypes have been PPAR α (primarily expressed in the liver and demonstrated to play a critical role in lipid metabolism) and PPAR γ (primarily expressed in adipose tissue and implicated in insulin sensitization as well as glucose and fatty acid utilization). PPAR α is the target of the fibrate class of hypolipidemic drugs such as fenofibrate (Balfour et al., 1990; Packard, 1998; Despres, 2001) and gemfibrozil (Spencer and Barradell, 1996), whereas PPAR γ is the target of the thiazolidinedione (Mudaliar and Herry, 2001) class of antidiabetic drugs such as rosiglitazone (Barman Balfour and Plosker, 1999; Cheng-Lai and Levine, 2000; Goldstein, 2000) and pioglitazone (Gillies and Dunn, 2000). Muraglitazar (*N*-[(4-methoxyphenoxy)carbonyl]-*N*-[[4-[2-(5-methyl-2-phenyl-4-oxazolyl)ethoxy] phenyl]methyl]glycine, BMS-298585, Pargluva, Figure 1), is an oxybenzylglycine analog (non-thiazolidinedione) dual α / γ PPAR activator currently in clinical development for the treatment of type 2 diabetes (Devasthale et al., 2005). This study describes the structural elucidation of oxidative metabolites of muraglitazar in humans following oral administration of [¹⁴C]muraglitazar through the use of a combination of microbial bioreactors, NMR, and accurate mass LC/MS.

The advantages of microbial bioreactors as a complementary *in vitro* system for drug metabolism are the relatively low cost, mild conditions, ease of use, potential for efficient conversion with a high yield of metabolites, scale-up

DMD 7153

capability, and a potential to reduce the use of animals. Microbial strains including the zygomycete fungus *Cunninghamella elegans* and the actinomycete *Saccharopolyspora hirsuta* have been used to study biotransformation and biosynthesis of several drugs and have shown the ability to produce oxidative metabolite profiles similar to those found in mammalian species (Ikeda et al., 1995; Zhang et al., 1995; Zhang et al., 1996a; Zhang et al., 1997). Some of these microbial biotransformation reactions are catalyzed by cytochrome P450 enzymes (Yang et al., 1997; Zhang et al., 1995; Zhang et al., 1996b). Therefore, microbial bioreactors should be useful for generation of metabolites in sufficient quantity to aid in structural elucidation of human metabolites by spectroscopic and chromatographic methods.

MATERIALS AND PROCEDURES

Materials. [^{14}C]Muraglitazar with a radiospecific activity of 10 $\mu\text{Ci}/\text{mg}$ and a radiochemical purity of 99.4% was synthesized in multiple steps from [^{14}C]phenol in a 20% overall yield at the Pharmaceutical Research Institute, Bristol-Myers Squibb. The structure of muraglitazar and the positions of ^{14}C labels are shown in Figure 1. PEG-400 was purchased from Sigma-Aldrich Co. (Milwaukee, WI). Trifluoroacetic acid (TFA) was purchased from EM Science (Gibbstown, NJ). Ecolite[®] liquid scintillation cocktail was purchased from PerkinElmer Life Sciences (Meriden, CT). Deuterated solvents D_2O , CD_3CN , and CDCl_3 (D 99.8%) were obtained from Cambridge Isotope Laboratories, Inc. (Andover, MA). All organic solvents and water were of HPLC grade. Microbial strains were purchased from American Type Culture Collections.

Sample collection and preparation. The study in human subjects had the Institutional Review Board approval and all subjects were required to give informed and written consent prior to participation of the study. Six healthy human subjects each received an oral dose of 10 mg (100 μCi) of [^{14}C]muraglitazar in PEG-400. Plasma (1, 4, 12, 24, and 48 h), urine (0-240 h), and feces (0-240 h) were collected. Plasma was collected in EDTA and pooled across the 6 subjects. The plasma (1 mL) was extracted with acetonitrile (3 volumes) and centrifuged at 2000xg for 10 min. The supernatant was saved and the pellet was extracted twice with acetonitrile (3 mL). The radioactivity extraction efficiency was >95%. The combined supernatants were evaporated to dryness by

evaporation under a stream of nitrogen. The residue was re-dissolved in 200 μ L acetonitrile:water (3:7) and centrifuged at 2000xg for 10 min before HPLC analysis. Urine and feces were collected for 0-240 h at 24-h intervals and the volume of urine and the weight of feces were determined for mass balance. Fecal paste was prepared and pooled from all samples collected up to 10 days across 6 subjects. Samples of pooled feces (1 g) were extracted by mixing with ethyl acetate (3 mL) and centrifuging at 2000xg for 10 min. The supernatant was saved and the pellet was extracted twice with ethyl acetate (3 mL). The extraction efficiency of radioactivity was 84.5%. The combined supernatants were evaporated to dryness by evaporation under a stream of nitrogen. The residue was re-dissolved in 200 μ L acetonitrile:water (3:7) and centrifuged at 2000xg for 10 min before HPLC analysis. Urine was concentrated directly under a stream of nitrogen. Plasma, urine, and fecal extracts were analyzed by HPLC separation, fraction collection, and radioactivity counting as well as by accurate mass LC/MS and LC/MS/MS.

Microbial incubations and isolation of metabolites. The fungus *Cunninghamella elegans* (ATCC 20230) and the actinomycete *Saccharopolyspora hirsuta* (ATCC 20501) were grown in 500-mL flasks at 28°C and 200 rpm in an rotary shaker on a medium consisting of 0.5% toasted nutrisoy, 2% glucose, 0.5% yeast extract, 0.5% K₂HPO₄, 0.5% NaCl, adjusted to pH 7 with aqueous HCl (Rosazza and Smith,1979). The bacterial strain was started from a 1 mL vial (stored in liquid nitrogen) in 100 mL medium grown for 3 days, then 10 mL of the culture from this flask was used to inoculate 100 mL

medium. The filamentous fungus were grown from a 1 mL spore suspension in 100 mL of medium. Muraglitazar (30 mg slurried in 1 mL methanol) was added to each flask after 24 h growth of the second stage bacterial culture or first stage fungal culture. The incubations were continued for 72 h, then the reactions were quenched with 100 mL of acetonitrile. After storage for several hours at room temperature and 4 days at 4°C, cells were removed by centrifugation at 3000xg for 10 min. A 50 mL portion of each supernatant was extracted twice with ethyl acetate (50 mL for each extraction). The combined ethyl acetate extracts were evaporated to near dryness under a stream of nitrogen. The residues were each reconstituted in 2 mL acetonitrile/water (3:7, v/v). The extracts were analyzed by accurate mass LC/MS and LC/MS/MS. For metabolite isolation, fractions were collected from 5 injections (100 µL) onto a 4.6x150 mm YMC HPLC column. The microbial isolates were analyzed by LC/MS, LC/MS/MS, and NMR.

Radioactivity detection. Radioactivity in the biological samples was determined by mixing an aliquot of the sample with 15 mL of Ecolite[®] cocktail and counting for 10 min using a Packard Tri-Carb 2250 liquid scintillation analyzer (PerkinElmer Life and Analytical Sciences, Boston, MA). The radioactivity in fecal homogenates was determined by combusting the samples followed by liquid scintillation counting. For HPLC profiling, the HPLC eluent was collected in 96-deep-well Lumaplates[®] and dried in a Speed-Vac[®] (Savant Instruments, Holbrook, NY). The plates were counted for 10 min per well using a TopCount[®] scintillation analyzer (PerkinElmer Life and Analytical Sciences, Boston, MA).

HPLC. HPLC was performed on a Shimadzu Class VP[®] system equipped with two pumps (model LC-10AT), an auto-injector (SIL 10AD), and a diode array detector (SPD-M10A) (Shimadzu, Kyoto, Japan). YMC ODS AQ C-18 columns (4.6 or 2.0 x 150 mm, 5 μ) were used for all separations. HPLC effluent fractions were collected into the 96-well plates at 0.26 min intervals for 70 min after sample injection with a Gilson Model 202 fraction collector (Gilson Medical Electronics, Middleton, WI). The columns were eluted with solvents A and B. Solvent A was water containing 0.06% TFA. Solvent B was acetonitrile containing 0.06% TFA. The initial conditions were 5% Solvent B. The B composition was increased linearly to 25% (5 min), 40% (15 min), 53% (40 min), 60% (3 min), and 90% (2 min), and then was held at 90% for 7 min. The flow rates were 1 mL/min for the 4.6 x 150 mm column and 0.3 mL/min for the 2.0 x 150 mm column. Metabolites in plasma, urine, and fecal extracts were monitored by radioactivity detection in collected fractions and metabolites in microbial incubations were monitored by on-line UV detection at 280 nm.

LC/MS and LC/MS/MS analyses. A YMC ODS AQ C-18 column (2.0 x 150 mm, 5 μ) was used for LC/MS. A Finnigan LCQ *deca* XP mass spectrometer with an ESI (+) source (ThermoFinnigan, San Jose, CA) was used for initial MS/MS analysis of fungal metabolites. The capillary temperature used for analysis was 230°C. The nitrogen gas flow rate, spray current, and voltages were adjusted to give maximum sensitivity for the parent compound. The collision energy was 20%. Accurate mass analysis was conducted on a Micromass Q-TOF Ultima mass spectrometer that was equipped with a Lock-Spray and an ESI(+) source

(Waters, Boston, MA). LC/MS/MS analysis of the human and microbial metabolites was also performed with the Q-TOF with the collision energy of 15-25%. The HPLC eluent was directed to the mass spectrometer. The desolvation temperature used for analysis was 300°C. The nitrogen gas flow rate, spray and cone voltages were adjusted to give maximum sensitivity for muraglitazar. The m/z 556.2771 of an infused 20 ng/ μ L leucine enkephalin solution was used as Lock Mass. The Q-TOF was tuned to 18,000 resolution at half peak height using an insulin tuning solution (at m/z 956.3), and was calibrated up to 1500 Da using a polyalanine calibration solution. The experimentally obtained masses matched their respective calculated values with an error of less than 5 mDa (<10 ppm).

NMR. The synthetic materials and microbial isolates were analyzed on a Jeol ECL-500 MHz spectrometer or a Bruker AVANCE 600 MHz system equipped with a 5 mm Z gradient probe, or a 3 mm Nalorac probe. 1D ^1H , 2D COSY (correlation spectroscopy), 2D TOCSY (total correlation spectroscopy), HMQC (one bond carbon-proton correlation), HMBC (long range carbon-proton correlation) and edited DEPT (enhancement by polarization transfer) experiments were performed. All chemical shifts are reported in ppm relative to tetramethylsilane in CD_3CN . For reference, a complete proton and carbon peak assignment of the NMR spectra was made on the parent drug.

Synthesis of M5. The proposed structure for M5 based on mass spectral analysis had a hydroxyl group on carbon-12. To confirm this structure, 12-

DMD 7153

hydroxy muraglitazar was synthesized in several steps (Figure 2A) as described below.

Intermediate 1: A solution of 4-hydroxybenzaldehyde (1.0 g, 8.2 mmol), tetrabutylsilyl chloride (TBSCl, 1.48 g, 9.8 mmol), and imidazole (660 mg, 9.8 mmol) in *N,N*-dimethylformamide (DMF, 10 mL) was stirred at room temperature for 3 h. The reaction mixture was then partitioned between ethyl acetate (EtOAc) and brine (saturated NaCl solution). The organic phase was washed with 10% aqueous lithium chloride, dried over anhydrous magnesium sulfate (MgSO₄), and concentrated under vacuum to give the TBS ether, which was used in the next step without further purification. A solution of the TBS ether, glycine methyl ester hydrochloride (1.23 g, 9.8 mmol), and triethylamine (Et₃N, 0.4 mL, 9.8 mmol) in methanol (MeOH, 20 mL) was stirred at room temperature for 18 h, and then sodium borohydride (NaBH₄, 370 mg, 9.8 mmol) was cautiously added portion-wise. The reaction was stirred for 1 h at room temperature followed by addition of saturated aqueous sodium bicarbonate (NaHCO₃) and removal of volatiles under vacuum. The residue was partitioned between EtOAc and saturated aqueous NaHCO₃. The organic phase was dried (MgSO₄) and concentrated under vacuum to give the amino ester intermediate **1** (1.3 g, 51%) as an oil, LC/MS [*M* + *H*]⁺ = 310. The oil was used in the next reaction without further purification.

Intermediate 2: A solution of amino-ester intermediate **1** (500 mg, 1.6 mmol), 4-benzyloxyphenyl chloroformate (510 mg, 1.9 mmol), and Et₃N (0.27 mL, 1.9 mmol) in methylene chloride (CH₂Cl₂, 10 mL) was stirred at room temperature for 2 h. The reaction mixture was then partitioned between CH₂Cl₂ and saturated

DMD 7153

aqueous NaHCO_3 . The organic phase was dried (MgSO_4) and concentrated under vacuum to give the desired carbamate ester, LC/MS $[\text{M} + \text{H}]^+ = 536$, which was used in the next step without further purification. To a solution of the TBS-ether carbamate ester in tetrahydrofuran (THF, 10 mL) was added tetrabutylammonium fluoride (Bu_4NF , 1.9 mL of a 1 M solution in THF, 1.9 mmol) at room temperature. The reaction was stirred for 1 h at room temperature, then was concentrated under vacuum. The residue was partitioned between ethyl acetate (EtOAc) and aqueous 1 N hydrochloric acid (HCl). The organic phase was dried (MgSO_4) and concentrated under vacuum. The residue was chromatographed on a silica gel column (stepwise gradient from 85:15 to 55:45 hexane:EtOAc) to give the phenol carbamate ester intermediate **2** (300 mg, 44%) as a clear oil, LC/MS $[\text{M} + \text{H}]^+ = 422$.

Intermediate **3**: A mixture of the phenol intermediate **2** (120 mg, 0.28 mmol), the mesylate intermediate **4** (which was prepared at Bristol-Myers Squibb, 100 mg, 0.24 mmol, Devasthale et al., 2005), and potassium carbonate (K_2CO_3 , 67 mg, 0.48 mmol) in acetonitrile (MeCN, 10 mL) was stirred at 90°C for 36 h. The reaction then was cooled to room temperature and stirred for 36 h. Volatile materials were removed under vacuum and the residue was partitioned between EtOAc and brine. The organic phase was dried (MgSO_4) and concentrated under vacuum to give the desired alkylated phenol as an oil, which was used in the next step without further purification.

A solution of the alkylated phenol in THF (5 mL) and Bu_4NF (0.50 mL of a 1 M solution in THF, 0.50 mmol) was stirred at room temperature for 15 min to give a

solution of the crude alcohol intermediate **3**, LC/MS $[M + H]^+ = 623$. Methanol (10 mL) and aqueous NaOH (2 mL of a 1 N solution) were added to the reaction mixture and the reaction was stirred at room temperature for 16 h. The solution was acidified with 1 N aqueous HCl, then was concentrated under vacuum. The residue was partitioned between EtOAc and 1 N aqueous HCl. The organic phase was dried ($MgSO_4$) and concentrated under vacuum. The residue was purified by preparative HPLC on a Phenomenex Luna C18 column (5 μ , 21.2 x 100 mm; detection at 220 nm; a flow rate = 25 mL/min; continuous gradient from 90% solvent A:10% solvent B to 100% solvent B over 8 min, where solvent A = 90:10:0.1 H_2O :MeOH:TFA and solvent B = 90:10:0.1 MeOH: H_2O :TFA) to give the O-benzylphenyl carbamate acid **3** (69 mg, 40%) as a white solid. LC/MS $[M + H]^+ = 609$.

Metabolite M5: To a solution of the O-benzylphenyl carbamate acid **3** in MeOH (10 mL) was added 10% palladium on carbon catalyst (50 mg) and the reaction was stirred under an atmosphere of hydrogen at room temperature for 30 min. After the catalyst was filtered off, the solution was concentrated under vacuum and the residue was purified as described for purification of the intermediate **3** to give metabolite **M5** (25 mg; 43%) as a white powder. LC/MS $[M + H]^+ = 519$. 1H NMR (400 MHz, CD_3OD): 7.91 (m, 2H), 7.40 (m, 3H), 7.15 (m, 2H), 6.82 (m, 4H), 6.67 (m, 2H), 4.58 (s, 2H), 4.47 (2s, 2H), 4.18 (t, $J = 6.5$ Hz, 2H), 3.89 (2s, 2H), 2.98 (t, $J = 6.5$ Hz, 2H).

Synthesis of M12. The proposed structure for M12 based on mass spectral analysis was oxidation of the methyl-12 to a carboxylic acid. To confirm this

structure, muraglitazar 12-carboxylic acid was synthesized in two steps (Figure 2B) as described below.

Aldehyde Intermediate: To an 8-mL screw cap vial was added muraglitazar (52.5 mg, 0.10 mmol), 1-hydroxy-1,2-benziodoxole-3(1*H*)-one-1-oxide (IBX, 281.0 mg, 1.0 mmol), dimethyl sulfoxide (DMSO, 4.0 mL) and a magnetic stir bar. The vial was capped and placed in an oil bath heated at 110°C for 24 h. The reaction mixture was diluted with 4.0 mL of acetonitrile and subjected to preparative HPLC isolation using a Phenomenex LUNA C18 column, 21.2 x 150 mm, 5 µm with solvent A (water with 0.05% trifluoroacetic acid) and solvent B (acetonitrile with 0.05% TFA). The linear gradient used was 50% B to 90% B in 10 min at a flow rate of 21.0 mL/min (monitored at 280 nm). Fractions containing the product were pooled, concentrated via rotary evaporation, and freeze-dried to afford an off-white powder (9.5 mg, 16% isolated yield). ¹H NMR (600 MHz, DMSO-*d*₆) 9.9 (s, 1H), 8.08 (d, *J* = 7.6 Hz, 2H), 7.63 (m, 1H), 7.58 (m, 2H), 7.26, 7.22 (d, *J* = 8.0 Hz, 2H, rotamers), 6.97 (m, 2H), 6.90 (m, 4H), 4.53, 4.39 (s, 2H, rotamers), 4.33 (m, 2H), 3.84, 3.79 (s, 2H, rotamers), 3.72 (s, 3H), 3.38 (m, 2H); ¹³C NMR (100 MHz, DMSO-*d*₆) 177.7, 170.7 and 170.4 (rotamers), 163.0, 157.5, 156.5, 154.8 and 154.5 (rotamers), 150.6, 145.7, 144.5, 132.4, 129.4 (4C), 129.0, 127.2 (2C), 125.4, 122.5 and 122.4 (rotamers, 2C), 114.6 and 114.5 (rotamers, 2C), 114.2 (2C), 65.2, 55.4, 50.8 and 50.7 (rotamers), 48.5 and 48.3 (rotamers), 26.3; HRMS (ESI+) calcd for C₂₉H₂₆N₂O₈Na ([M+Na]⁺): 553.1587; found: 553.1575.

DMD 7153

Metabolite **M12**. The reaction was carried out by mixing a sample of the aldehyde intermediate (9.0 mg) in 0.2 mL DMSO and 1-hydroxy-1,2-benziodoxole-3(1*H*)-one-1-oxide (IBX, 7.6 mg) and N-hydroxysuccinimide (9.8 mg). The reaction proceeded very slowly at ambient temperature, but achieved total conversion at 80°C for 24 h. The reaction mixture (about 0.14 mL) was diluted with acetonitrile (1.0 mL) and water (0.5 mL). The resulting solution was used for product isolation via semi-preparative HPLC using a Phenomenex LUNA C18 column, 10 x 150 mm, 5 μ with solvent A (5% acetonitrile/95% water with 0.01M NH₄OAc) and solvent B (95% acetonitrile/5% water with 0.01M NH₄OAc). The linear gradient used was 10% B to 70% B in 20 min at a flow rate of 4.7 mL/min (monitored at 280 nm). Fractions containing the product were pooled, concentrated via rotary evaporation, and freeze-dried to afford a white powder (ca. 1 mg). ¹H NMR (600 MHz, DMSO-d₆) 7.96 (d, *J* = 6.6 Hz, 2H), 7.50 (m, 3H), 7.25 and 7.21 (d, *J* = 8.2 Hz, 2H, rotamers), 6.89-7.00 (m 6H), 4.54 and 4.40 (s, 2H, rotamers), 4.26 (t, *J* = 7.3 Hz, 2H), 3.88 and 3.63 (s, 2H, rotamers), 3.72 (s, 3H), 3.29 (t, *J* = 7.3 Hz, 2H); HRMS (ESI+) calcd for C₂₉H₂₇N₂O₉ ([M+H]⁺): 547.1717; found: 547.1727.

RESULTS

Biotransformation profiles in human plasma, urine, and feces and in microbial incubations

Following oral administration of [¹⁴C]muraglitazar (10 mg) to humans, urinary excretion was very minimal (3.5% of the dose) and the majority of radioactivity

was excreted in feces (approximately 96% of the recovered radioactive dose). The overall radioactivity recovery was low (64%) from this study, possibly due to difficulties in accurately measuring the radioactivity in a fecal paste preparation. An additional human ADME study showed >93% recovery of the radioactive dose in which feces was homogenized in a water and ethanol mixture. The fecal metabolite profile was similar in both studies (data not shown). Figure 4 shows the HPLC-radioactivity profiles of selected human plasma samples. The parent compound represents >90% of the radioactivity in human plasma at early time points, and >85% at 48 h. No metabolites accounted for >5% of the radioactivity in plasma at any time point. Human metabolites identified in plasma included M18, M5, M10, M11, M13, and M15. Figure 5 shows metabolite profiles of human feces (by radioactivity) and microbial incubations (by UV at 280 nm). Four metabolite peaks (M5, M10, M11, and M15) and P were the major radioactive components in human feces and together accounted for >70% of the radioactivity in the fecal sample (Figure 5). Human urine contained several radioactive peaks including M13 and the parent compound (P) with M13 accounting for approximately 1% of the dose. Figure 6 shows the selected ion chromatographic profiles of muraglitazar metabolites in human feces. There were four hydroxy metabolites (M8a, M10, M11, and M14), four hydroxy O-demethyl metabolites (M2, M5, M6, and M7), one O-demethyl metabolite (M15), three dihydroxy metabolites (M3, M4, and M8), one dioxygenation with dehydrogenation metabolite (M12), and two oxazole ring-opening metabolites (M9 and M16). Because human feces, as the major excretion route, contained low

concentrations of metabolites of muraglitazar at a 10 mg dose, detailed structural identification of fecal metabolites through isolation was not practical. Microbial bioreactors were thus used to generate sufficient quantities for isolation and identification of the human metabolites. Microbes *S. hirsuta* and *C. elegans* produced high yields of metabolites which had the same retention times as human fecal metabolites M9, M10, M11, M14, M15 and M16 (Figure 4). In addition to these major metabolites, the microbial strains also produced other oxidative metabolites that had the same retention times and fragmentation patterns as those found in human feces (partial data were shown in Table 2). Comparative HPLC/accurate MS chromatographic profiles were very similar between in human feces and microbial incubations for selected muraglitazar metabolites as demonstrated in Figure 5. In addition, the mass spectral fragmentation patterns and molecular formula calculated with a 5 ppm accuracy of these microbial metabolites matched the corresponding human metabolites (Table 2). Based on these comparisons, the microbial metabolites were judged to be identical to the human metabolites.

Identification of metabolites

Typical fragmentation patterns of muraglitazar in a full scan MS analysis showed cleavage at the benzylic C-N bond adjacent to carbamate (C3-N) to give a fragment at m/z 292 and cleavage at the ether bond (C8-O) to give a fragment at m/z 186 (as shown in Figure 1). Muraglitazar had a molecular ion $[M+H]^+$ at m/z 517 (Table 2). The key 1H NMR data (Table 3) for metabolite identification are

the chemical shifts (ppm) at 2.35 for the methyl group at position 12, 2.92 for the methylene at position 9, 3.77 for the methoxy group at position 23, and 7.47 or 7.48 for the aromatic protons at positions 16 and 17.

Similar fragmentation patterns were observed with muraglitazar metabolites M2-M16. All mono-hydroxylation metabolites (M2, M5, M6, M7, M8a, M10, M11, and M14) showed a fragmentation ion at m/z 202 ($186+16$) or its dehydrated form at m/z 184 ($202-H_2O$), indicating that oxygen addition occurred on the oxazole-ring side of the molecules. Mono-hydroxylation metabolites, M2, M5, M7, M8a, M10, and M14 (but not M6 and M11 which were hydroxylated at position 17), also showed a fragmentation ion at m/z 187.0756, which had a formula of $C_{12}H_{11}O_2$, indicating that the nitrogen was lost in the mass spectrometer after ether cleavage of the oxygenated molecules ($187=186-NH+oxygen$). The mechanism for this gas phase reaction is not currently understood. NMR data of metabolites were analyzed by comparison to the spectra of the parent muraglitazar. Metabolites M9, M10, M11, M14, M15, and M16 were isolated from incubations with *C. elegans* and *S. hirsuta* and identified by NMR and LC/MS/MS analyses. The structures of other human metabolites were identified by comparing their MS/MS spectra with those metabolites identified by NMR. M5 and M12 were synthesized as reference standards following preliminary identification by LC/MS/MS analysis.

Metabolites M8a, M10, M11, and M14 (mono-hydroxylated metabolites): These four metabolites had the same molecular ion $[M+H]^+$ at m/z 533. They all had similar fragmentation patterns to each other and to the parent compound,

DMD 7153

cleaving at the C8-O and C3-N bonds (Figure 6A). Their MS/MS spectra suggested that the hydroxylation was on the oxazole-ring side of the molecules.

Metabolite M11 showed fragments at m/z 308 (cleavage at the C3-N bond), and 202 (cleavage at the C8-O bond) (Figure 6A). The proton 1D NMR spectrum (Figure 7A) of the microbial isolate showed that this metabolite had two characteristic changes with respect to the parent drug. These changes were: 1) absence of a signal for the proton at position 17 and 2) a significant upfield shift of the protons at position 16, from 7.48 ppm to 6.92 ppm. The signals for the protons at position 15 also showed a small shift from 7.94 ppm to 7.80 ppm. These results indicated that the hydroxylation was at the para-position 17, and metabolite M11 was thus assigned as 17-hydroxy muraglitazar.

Metabolite M10 showed fragment ions at m/z 308 (cleavage at the C3-N bond), 290 ($290=308-H_2O$), 202 (cleavage at the C8-O bond), and 184 ($184=202-H_2O$) (Figure 6A). The fragment ion at m/z 278 ($278=292+16-30$) was consistent with the loss of formaldehyde from cleavage at the C3-N bond. The proton 1D NMR spectrum (Figure 7A) of the microbial isolate showed the absence of the methyl signal at 2.35 ppm, and the appearance of a new signal at 4.6 ppm (a singlet integrating for 2 protons, characteristic of a CH_2OH group). All other protons could be accounted for. These results indicated that the hydroxylation was at position 12 (oxazole-methyl group), and metabolite M10 was thus assigned as 12-hydroxy muraglitazar.

Metabolite M14 showed fragment ions at m/z 290 (cleavage at the C3-N bond, $290=308-H_2O$) and 202 (cleavage at the C8-O). The proton 1D NMR spectrum (Figure 7A) showed that the proton 9 resonance of this metabolite had a dramatic downfield shift from 2.92 ppm to 5.04 ppm. This signal was still a triplet and couples (in the 2D TOCSY spectrum) to the signal at 4.27 ppm of proton 8. Even so, there was no significant shift on the resonance frequency of proton 8 relative to the parent drug. Proton 8 was no longer a triplet, but rather a broad doublet, supporting that it was coupling to only one other proton. These results indicated that the hydroxylation was on position 9, and metabolite M14 was thus assigned as 9-hydroxy muraglitazar. The absolute stereochemistry of M14 is not known.

Metabolite M8a showed fragment ions at M/Z 308 (cleavage at the C3-N bond) and 187 (cleavage at the C8-O bond). The absence of the ether cleavage fragment at m/z 202 observed with other hydroxy metabolites indicated the instability of this fragment in the mass spectrometer. The result suggested that the hydroxylation was probably at position 8 (methylene group). This hemiacetal structure was expected to have some degree of instability in aqueous environments, which was consistent with the low concentration of this metabolite in human feces and the subsequent formation of the *O*-dealkyl metabolite M1. Although the position for the hydroxyl group in M8a was not determined, available data supported a tentative assignment for M8a as 8-hydroxy muraglitazar.

Metabolite **M15**: M15 showed a molecular ion $[M+H]^+$ at m/z 503 and major fragment ions at m/z 186 and 292 in the LC/MS analysis, consistent with *O*-

demethylation. ^1H and ^{13}C NMR analyses showed that M15 lacked the OCH_3 group (at 3.8 ppm for ^1H in Figure 7B and 55 ppm for ^{13}C) observed for the parent muraglitazar. The only change was the disappearance of the methoxy resonance of position 23. All other signals were in the same range as in the parent molecule, including the ortho- and meta- positions in the corresponding aromatic ring (Table 3, Figure 7B). This metabolite was assigned as O-demethyl muraglitazar.

Metabolites M9 and M16: These two metabolites had mass spectral characteristics distinct from muraglitazar and other metabolites. They showed a strong Na adduct of the molecular ions in LC/MS analyses. Both of these metabolites did show typical fragmentation patterns, cleaving at the C8-O and C3-N bonds.

Metabolite M9 had a molecular ion $[\text{M}+\text{H}]^+$ at m/z 507 (loss of 10 Da from the parent compound) and fragment ions at m/z 282 (cleavage at the C3-N bond, $282=292-10$) and 176 (cleavage at the C8-O bond, $176=186-10$). Accurate mass analysis and formula calculation indicated that the 10 Da loss was due to elemental composition changes with an addition of oxygen and loss of ethylene ($+\text{O}-\text{C}_2\text{H}_2$). The UV spectral changes (from a strong absorption peak around 250-315 nm and a weak absorption peak around 210-240 nm to a strong absorption peak around 200-255 nm and a weak absorption peak around 265-285 nm) suggested the removal of the extended aromatic system, consistent with oxazole ring opening. The proton 1D NMR spectrum (Figure 7B) showed that the methyl resonance at position 12 was lost and there was no new signal that could

account for these protons, suggesting that this position was not simply hydroxylated. These results indicated that the metabolite had an oxazole ring opening structure. Metabolite M9 was assigned as the oxazole ring-opening imide derivative of muraglitazar.

Metabolite M16 showed a molecular ion $[M+H]^+$ at m/z 549 (plus 32 Da from the parent compound) and fragment ions at m/z 324 (cleavage at the C3-N bond, $324=282+42$, an acetyl group), 282 (cleavage at the C3-N bond, $282=292-10$), 218 (cleavage at the C8-O bond, $218=176+42$, an acetyl group), and 176 (cleavage at the C8-O bond, $176=186-10$). This fragmentation pattern suggested that M16 was a derivative of M9 with the addition of an acetyl group. The proton 1D NMR spectrum showed a new signal in the aliphatic region at 2.28 ppm that might be attributed to an acetyl group (not shown). A theoretical prediction of the NMR spectrum of this proposed structure gave a value of 2.24 ppm for the acetyl group, in good agreement with the experimental value. These results supported that this metabolite was an *N*-acetyl derivative of M9, and metabolite M16 was thus assigned as oxazole ring-opening *N*-acetylimide derivative of muraglitazar.

Metabolites **M2**, **M5**, **M6**, and **M7** (O-demethylated and hydroxylated metabolites): These four metabolites had the same molecular ion $[M+H]^+$ at m/z 519 ($519=517+16-14$), consistent with hydroxylation and O-demethylation. They had typical fragmentation patterns of cleavage at either the C8-O or the C3-N bond (Figure 6B). Their MS/MS spectra also suggested that the hydroxylations were on the oxazole-ring side of the molecules. M2, M5, M6, and M7 had the same fragmentation patterns as monohydroxy metabolites M8a, M10, M11, and

M14, respectively. Therefore, these compounds were assigned as the O-demethylation metabolites corresponding to the hydroxy metabolites M8a, M10, M11, and M14. M2 was tentatively assigned as 8-hydroxy O-demethyl muraglitazar. Similar to the assignment for M8a, available data supported the hydroxyl group at C8 although the final structure for M2 was not determined. M5 was assigned as 12-hydroxy O-demethyl muraglitazar. M6 was assigned as 17-hydroxy O-demethyl muraglitazar. M7 was assigned as 9-hydroxy O-demethyl muraglitazar.

The synthesis of the metabolite M5 is outlined in Figure 2A. 4-Hydroxybenzaldehyde was protected as the t-butyldimethylsilyl ether, then was subjected to reductive amination with glycine methyl ester hydrochloride to give the secondary amine **1**. Acylation of amine **1** with 4-benzyloxyphenyl chloroformate, followed by deprotection of the tert-butyldimethylsilyl ether, furnished the phenol carbamate-ester **2**. Alkylation of phenol **2** with the hydroxylated phenyloxazole mesylate **4**, followed by deprotection of the TBS ether, provided the hydroxymethyl oxazole carbamate-ester **3**. Deprotection of **3** (hydrogenolysis of the O-benzyl ether followed by ester hydrolysis) provided the metabolite M5. Synthetic M5 had the same HPLC retention time and MS/MS fragmentation patterns as the corresponding metabolites from human feces (data not shown).

Metabolites M3, M4, M8, and M12: Metabolites M3, M4, and M8 had the same molecular ion $[M+H]^+$ at m/z 549 ($549=517+32$), which was consistent with dihydroxylation. Metabolite M12 had a molecular ion $[M+H]^+$ at m/z 547

($549=517+32-2$), which was consistent with dioxygenation and dehydrogenation. All of these metabolites showed a typical fragmentation pattern, with cleavage at the C8-O and C3-N bonds (Table 2 and Figure 6C). The MS/MS spectra for all the metabolites suggested that both hydroxylations were on the oxazole ring side of the molecules.

Metabolite M4 showed fragment ions at m/z 531 ($549-H_2O$), 324 (cleavage at the C3-N bond, $324=292+16+16$), 306 ($306=324-H_2O$), 218 (cleavage at the C8-O bond, $218=186+16+16$), and 200 ($200=218-H_2O$) (Figure 6C). This was a similar fragmentation pattern to that of the 12-mono-hydroxylation metabolite M10 (Table 2 and Figure 6A). In addition, M4 had a characteristic fragment at m/z 294, loss of formaldehyde (from cleavage at the C3-N bond, $294=324-CH_2O$); this fragmentation was also observed in the 12-hydroxy metabolites M5 and M10 (at m/z 278). M4 also showed a characteristic fragment at M/Z 192.0687 ($C_{10}H_{10}NO_3$), which could be formed from the cleavage between the C-9 and C-10 bond followed by a hydration. These results suggested dihydroxylation at the 9 and 12 positions. Metabolite M4 was tentatively assigned as 9,12-dihydroxy muraglitazar.

Metabolite M8 showed fragment ions at m/z 324 (cleavage at the C3-N bond, $324=292+16+16$) and 218 (cleavage at the C8-O bond, $218=186+16+16$) (Figure 6C). The fragmentation pattern was similar to that of 17-hydroxy muraglitazar except for the additional 16 mass unit increase for each fragment. M8 was tentatively assigned as 12,17-dihydroxy muraglitazar. Although another possibility could be that the second hydroxylation occurs on the same phenyl ring

(16,17-dihydroxy muraglitazar), a trace level of a fragment at m/z 306 ($306=324-H_2O$) in the MS/MS of M8 suggested that M8 was more likely to be 12,17-dihydroxy muraglitazar.

Metabolite M3 showed fragment ions at m/z 324 (cleavage at the C3-N bond, $324=292+16+16$), 187 (cleavage at the C8-O bond, $C_{12}H_{11}O_2$), and 192 ($C_{10}H_{10}NO_3$) (Figure 6C). Detection of the fragment ion at m/z 187 ruled out the possibility for 17-hydroxylation. No other major fragment ions were observed with this metabolite. The result suggested dihydroxylation at position 8 and 12. M3 was tentatively assigned as 8,12-dihydroxy muraglitazar.

Metabolite M12 showed fragments at m/z 322 (cleavage at the C3-N bond, $324=292+16+16-2$) and 218 (cleavage at the C8-O bond, $218=186+16+16-2$) (Figure 6C). One structure that was consistent with these observations was muraglitazar 12-carboxylic acid. Other structures including 12-oxa-17-hydroxy muraglitazar, 9-oxa-17-hydroxy muraglitazar, 12-oxa-9-hydroxy muraglitazar could not be ruled out. To confirm the structure of M12, muraglitazar 12-carboxylic acid was synthesized with a two-oxidation steps from muraglitazar. Literature procedures for the oxidation of a methyl group that is directly attached to an oxazole ring to an aldehyde and from an aldehyde to a carboxylic acid were used for the preparation (Nicolaou et al., 2001; Mazitschek et al., 2002). Synthetic M12 had the same HPLC retention time and MS/MS fragmentation patterns as the corresponding metabolites from human feces (data not shown).

Metabolites **M13 and M18**: A very trace level of M13 was detected in human fecal extract by LC/MS/MS, however, this was a relatively major metabolite in human urine. This metabolite had a molecular ion $[M+H]^+$ at m/z 693 and fragment ions at m/z 517, 292, and 186 (the same fragment ions as muraglitazar), consistent with an acyl glucuronide of the parent compound. M13 was tentatively assigned as an acylglucuronide of muraglitazar. M18 was a minor metabolite detected in plasma and urine. M18 had a molecular ion $[M+H]^+$ at m/z 709 and fragment ions of 533, 308, and 202, consistent with a glucuronide of hydroxy muraglitazar. M18 was assigned as the glucuronide of an isomer of hydroxy muraglitazar although the position for the glucuronic acid was not determined.

Metabolite **M1**: This peak was a minor metabolite in human feces (Figure 3). The radioactive peak had the same retention time as a metabolite in microbial incubations. Based LC/MS and LC/MS/MS analyses, M1 was tentatively assigned as O-dealkyl muraglitazar.

DISCUSSION

Following oral administration of $[^{14}C]$ muraglitazar to healthy subjects, the parent drug was the major radioactive component in the circulation. No single metabolite accounted for >5% of the total plasma radioactivity. Muraglitazar acyl glucuronide, M13, accounted for approximately 1% of the dose in urine. Fecal excretion represented >96% of the recovered radioactivity. Major fecal metabolites included M5, M10, M11, and M15. The parent drug accounted for

approximately 15% of the recovered radioactive dose in feces, while oxidative metabolites accounted for the remaining dose. All together, sixteen oxidative and two glucuronide metabolites were identified from plasma, urine, and feces. Muraglitazar and structurally characterized metabolites represented >95% of the radioactivity in excreta. The oxidative metabolites of [^{14}C]muraglitazar in human feces were probably generated by intestinal and liver CYP enzymes followed by biliary excretion. An additional mechanism could include intestinal excretion of metabolites. It is unlikely that the fecal metabolites were generated by the enzymes in the intestinal microflora as these enzymes are generally reductive in nature. Consistent with these findings, incubation of [^{14}C]muraglitazar in human liver microsomes in the presence of NADPH generated M1, M9, M10, M11, M12, M14, M15, and M16 as prominent oxidative metabolites (Data not shown). Although CYP enzymes are expected to catalyze formation of the initial oxidation product at C-12 of muraglitazar (M10) and other oxidative metabolites, the additional oxidation steps of the hydroxyl group in M10 to a carboxylic acid group in M12 could be catalyzed by an alcohol dehydrogenase and an aldehyde oxidase.

During the development of new chemical entities, there are two general questions regarding metabolite identification that need to be addressed. The first concern is which metabolites (above what concentration or what percent of the dose) should be structurally characterized and the second concerns the degree of characterization which is necessary for the metabolites. At the compound selection and optimization stage, only major metabolites and potentially toxic

and/or reactive metabolite(s) need to be identified to avoid compounds that may have unacceptable high clearance values or have the potential to cause toxicity through reactive metabolite generation. However, radioactive materials are often not available at this time and quantitation is often limited to estimation based on LC/UV detection. Minor metabolites are often missed by UV detection at this stage. Once in the development stage, ADME data in animals and humans with radiolabeled materials will reveal the major circulating metabolite(s) and major clearance pathways. The ADME data will also define relative concentrations of each metabolite in plasma, urine, bile, and feces. Since one of the main objectives for metabolism studies is to support drug safety evaluation studies, the Metabolite In Safety Testing (MIST) committee suggested that any circulating metabolites and any significant metabolites in excreta of humans should be characterized to understand the formation pathways of metabolites (Baillie et al., 2002). Identification of the major metabolites in human excreta not only aids in defining the major clearance pathways but also in the design of drug-drug interaction studies. Major metabolites in animals, which may not be important as human metabolites, should be also identified since they may explain the species specific toxicities observed in animals. Thus, there is a need to identify quantitatively and qualitatively important radioactive metabolites in studies with radiolabeled materials.

The structural identification of metabolites can be carried out at multiple levels. The goal of initial identification of metabolites is often accomplished through LC/UV, LC/MS, and LC/MS/MS analyses to determine the biotransformation

pathways involved in the clearance of the compound. Determination of the nature of the metabolites such as oxygenation (hydroxylation or oxidation of a heteroatom), dioxygenation, dealkylation, and conjugation (glucuronide, sulfate, glutathione etc) is often sufficient. The identification of metabolites from biological matrices beyond this initial level is often challenging. Due to low concentrations and interference from endogenous components, identification of metabolites with unusual structures presents additional challenges. Neutral loss and product ion scans have been used for real-time, data-dependent acquisition of full MS/MS data of expected metabolites to improve the selectivity and sensitivity (Castro-Perez et al., 2002). We have employed accurate mass spectrometry in this study for the analysis of the metabolite profile of muraglitazar in human feces. The accurate mass measurements not only provided cleaner selective ion chromatograms (ion chromatograms extracted with a mass accuracy to the second decimal places, Figures 3 and 4) of metabolites in feces but also provided spectra for easy identification of the molecular ions, which greatly enhanced the metabolite identification. Further refinement of this concept led to the development of a general mass defect filtering (MDF) methodology (Zhang et al., 2003). Consequently, MDF can be used to aid in the identification molecular ions of metabolites with unusual structures or present at low concentrations as well as for metabolites formed from expected biotransformations.

LC/MS and LC/MS/MS methods will often leave significant ambiguity in the exact structural identification of metabolites. The next level of identification involves detailed structural elucidation of the metabolites by NMR and often requires

quantities of materials not available from *in vivo* samples. In this study, we have demonstrated the use of microbial bioreactors to produce large quantities of major metabolites of muraglitazar for isolation and identification. Another major human metabolite, M5, was not produced in a sufficient quantity from the microbial incubations for isolation; however, the hydroxylation site in M5 was tentatively assigned from the isolation and partial identification of the microbial metabolite, which directed organic synthesis of the metabolite. The synthetic compound matched the human metabolite both by HPLC retention time and LC/MS and LC/MS/MS analyses.

In summary, the oxidative biotransformation pathways of muraglitazar in humans include hydroxylation, O-demethylation, hydroxylation/O-demethylation, oxazole-ring opening, O-dealkylation, and carboxylic acid formation. A combination of microbial bioreactors, NMR and LC/accurate mass analyses, and organic synthesis helped to successfully identify human fecal metabolites following oral administration of [¹⁴C]muraglitazar. Microbial bioreactors proved to be extremely useful as a source for oxidative metabolites of muraglitazar and greatly aided in metabolite identification. This methodology should be broadly applicable to the determination of metabolite structures for other new chemical entities.

Acknowledgements. We thank Dr. Jianmin Ren for review of the manuscript and Dr. Carl E Cerniglia from National Center for Toxicological Research for helpful discussions.

REFERENCES

Baillie TA, Cayen MN, Fonda H, Gerson RJ, Green JD, Grossman SJ, Klunk LJ, LeBlanc B, Perkins DG, and Shipley LA (2002) Contemporary issues in toxicology. Drug metabolites in Safety testing. *Toxicol Applied Pharmacol* **182**: 188-196.

Balfour JA, McTavish D, and Heel RC (1990) Fenofibrate. A review of its pharmacodynamic and pharmacokinetic properties and therapeutic use in dyslipidaemia. *Drugs* **40(2)**: 260-290.

Balfour JA, and Plosker GL (1999) Rosiglitazone. *Drugs* **57(6)**: 921-930.

Castro-Perez J, Hoyes J, Major H, and Preece S (2002) *Chromatographia* **55**: s59.

Cheng-Lai A, and Levine A (2000) Rosiglitazone: an agent from the thiazolidinedione class for the treatment of type 2 diabetes. *Heart Dis* **2(4)**: 326-333.

Despres JP (2001) Increasing high-density lipoprotein cholesterol: an update on fenofibrate. *Am J Cardiol* **88(12A)**: 30N-36N.

Devasthale PV, Chen S, Jeon Y, Qu F, Shao C, Wang W, Zhang H, Cap M, Farrelly D, Golla R, Grover G, Harrity T, Ma Z, Moore L, Ren J, Seethala R, Cheng L, Sleph P, Sun W, Tieman A, Wetterau JR, Doweiko A, Chandrasena G, Chang SY, Humphreys WG, Sasseville VG, Biller SA, Ryono DE, Selan F, Hariharan N, and Cheng PTW (2005) Design and synthesis of *N*-[(4-methoxyphenoxy)carbonyl]-*N*-[[4-[2-(5-methyl-2-phenyl-4-oxazolyl)ethoxy]phenyl]methyl]glycine, muraglitazar /BMS-298585], a novel peroxisome proliferator-activated receptor α/γ dual agonist with efficacious glucose and lipid-lowering activities. *J Med Chem* **48**: 2248-2250.

Goldstein BJ (2000) Rosiglitazone. *Int J Clin Pract* **54(5)**: 333-337.

Gillies PS, and Dunn CJ (2000) Pioglitazone. *Drugs* **60(2)**: 333-343 and 344-345.

Ikeka Y., Kondo S, Kanai F, Sawa T, Hamada M, Takeuchi T, and Umezawa H (1995) A new destomycin-family antibiotic produced by *Saccharopolyspora hiruta*. *J Antibiot (Tokyo)* **38**: 430-438.

Mazitschek R, Mulbaier M, and Giannis A (2002) IBX-mediated oxidation of primary alcohols and aldehydes to form carboxylic acids. *Andrew Chem Int Ed* **41(21)**: 4059-4061.

Mudaliar S, and Henry RR (2001) New oral therapies for type 2 diabetes mellitus: The glitazones or insulin sensitizers. *Annu Rev Med* **52**: 239-257.

Nicolaou KC, Barran PS, and Zhong YL (2001) Selective oxidation at carbon adjacent to aromatic systems with IBX. *J Am Chem Soc* **123**: 3183-3185.

Packard KA, Backes JM, Lenz TL, Wurdeman RL, Destache C, and Hilleman DE (2002) Comparison of gemfibrozil and fenofibrate in patients with dyslipidemic coronary heart disease. *Pharmacotherapy* **22**(12):1527-1532.

Rosazza JP and Smith RV (1979) Microbial models for drug metabolism. *Adv App. Microbiol* **25**:169-203.

Spencer CM, and Barradell LB (1996) Gemfibrozil. A reappraisal of its pharmacological properties and place in the management of dyslipidaemia. *Drugs* **51**(6): 982-1018.

Taskinen MR (2003) Diabetic dyslipidaemia: from basic research to clinical practice. *Diabetologia* **46**(6): 733-749.

Yajima H, Ikeshima E, Shiraki M, Kanaya T, Fujiwara D, Odai H, Tsuboyama-Kasaoka N, Ezaki O, Oikawa S, and Kondo K (2004) Isohumulones, bitter acids derived from hops, activate both peroxisome proliferator activated receptor alpha and gamma and reduce insulin resistance. *J Biol Chem* **279**(32): 33456-33462.

Yang YF, Zhang DL, and Cerniglia CE (1997) Purification and characterization of a soluble cytochrome P450 enzyme from yeast *Trichosporon cutaneum*. *FEMS Microbiol. Lett* **154**: 347-353.

Zhang DL, Evans FE, Freeman JP, Duhart B, and Cerniglia CE (1995) Biotransformation of the amitriptyline by *Cunninghamella elegans*. *Drug Metab Dispos* **23**: 1417-1425.

Zhang DL, Evans FE, Freeman JP, Yang YF, Deck JD, and Cerniglia CE (1996a) Formation of mammalian metabolites of cyclobenzaprine by the fungus, *Cunninghamella elegans*. *Chem Biol Interact* **102**: 79-92.

Zhang DL, Yang YF, Leakey J, and Cerniglia CE (1996b) Phase I and Phase II enzyme produced by *Cunninghamella elegans* for metabolism of xenobiotics. *FEMS Microbiol Lett* **138**: 221-226.

Zhang DL, Hansen EB, Deck JD, Heinze TM, Luneau A, Korfmacher WA, and Cerniglia CE (1997) Fungal transformation of antihistamines: metabolism of cyproheptadine hydrochloride by *Cunninghamella elegans*. *Xenobiotica* **27**: 301-315.

Zhang, HY, Zhang DL, and Ray K (2003) A software filter to remove interference ions from drugs metabolites in accurate mass liquid chromatography/mass spectrometric analyses. *J. Mass Spectrom* **38**: 1110-1112.

Legends for Figures

- Figure 1 Structure of muraglitazar with numbering system and major ESI(+)/MS fragmentation patterns.
- Figure 2 Synthetic scheme of metabolite M5, 12-hydroxy O-demethyl muraglitazar and M12, muraglitazar 12-carboxylic acid.
- Figure 3 HPLC profiles of muraglitazar metabolites in human feces and microbial incubations. Top panel represents metabolite profiles in feces by radioactivity and bottom two panels represent metabolite profiles in microbial bioreactors by UV at 280 nm. M1, M2, etc. represent muraglitazar metabolites and P represents muraglitazar. Only the major metabolites in the microbial metabolite profiles were labeled.
- Figure 4 Accurate LC/MS ion chromatographic profiles of [^{14}C]muraglitazar metabolites in human feces (A) oxazole-ring opening metabolite M9, (B) dioxygenation and dehydrogenation metabolite M12, (C) N-acetyl oxazole-ring opening metabolite M16, (D) the parent drug, (E) dihydroxylation metabolites M3, M4, and M8, (F) O-demethylation metabolite M15, (G) hydroxylation and O-demethylation metabolites M2, M5, M6, and M7, (H) hydroxylation metabolites M8a, M10, M11, and M14, and (I) radiochromatogram of human feces for comparison purpose. Ion chromatograms ($[\text{M}+\text{Na}]^+$ for M9 and M16 and $[\text{M}+\text{H}]^+$ for other metabolites) were

extracted with narrow mass ranges (0.1700-0.2200 Da) of metabolites and parent drug from accurate mass analyses.

Figure 5 Comparative Accurate LC/MS ion chromatographic profiles of muraglitazar metabolites: (A) and (B) oxazole-ring opening metabolite M9 in *C. elegans* and human feces, (C) and (D) N-acetyl oxazole-ring opening metabolite M16 in *S. hirsuta* and human feces, (E) and (F) O-demethylation metabolite M15 in *S. hirsuta* and human feces, and (G) and (H) hydroxylation metabolites M8a, M10, M11, and M14 in *S. hirsuta* and human feces. Ion chromatograms ($[M+Na]^+$ for M9 and M16 and $[M+H]^+$ for other metabolites) were extracted with narrow mass ranges (0.1700-0.2200 Da) of metabolites and parent drug from accurate mass analyses.

Figure 6 Q-TOF MS/MS spectra of human fecal metabolites of muraglitazar: (A) hydroxylation metabolites M14, M11, M10, and M8a, (B) hydroxylation/ O-demethylation metabolites M7, M6, M5, and M2, and (C) dihydroxylation metabolites M3, M4, and M8 and 12-carboxylic acid metabolite M12.

Figure 7 Proton 1D NMR spectra of microbial isolates of muraglitazar metabolites: (A) M10, M11, and M14, (B) M15, and M9.

Table 1. Proposed structures of muraglitazar metabolites

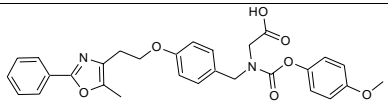
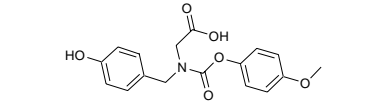
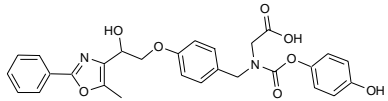
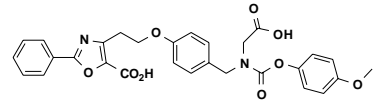
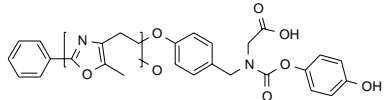
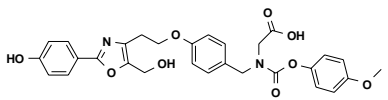
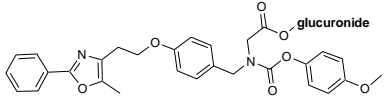
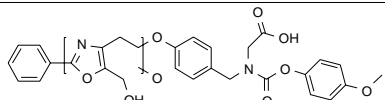
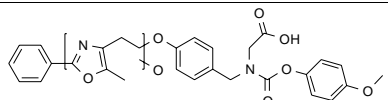
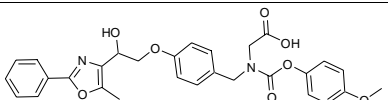
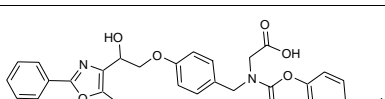
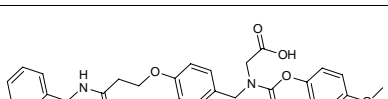
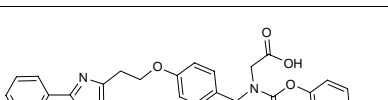
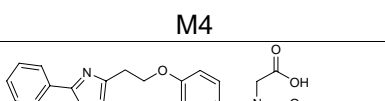
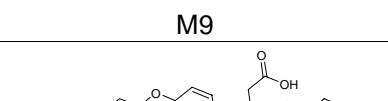
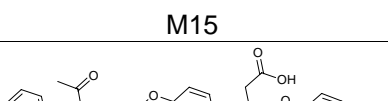
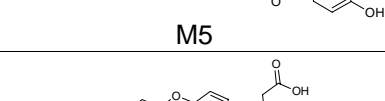
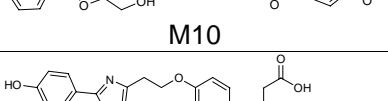
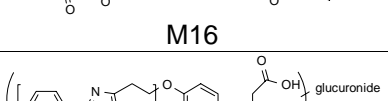
 <p style="text-align: center;">Muraglitazar</p>		
 <p style="text-align: center;">M1</p>	 <p style="text-align: center;">M7</p>	 <p style="text-align: center;">M12</p>
 <p style="text-align: center;">M2</p>	 <p style="text-align: center;">M8</p>	 <p style="text-align: center;">M13</p>
 <p style="text-align: center;">M3</p>	 <p style="text-align: center;">M8a</p>	 <p style="text-align: center;">M14</p>
 <p style="text-align: center;">M4</p>	 <p style="text-align: center;">M9</p>	 <p style="text-align: center;">M15</p>
 <p style="text-align: center;">M5</p>	 <p style="text-align: center;">M10</p>	 <p style="text-align: center;">M16</p>
 <p style="text-align: center;">M6</p>	 <p style="text-align: center;">M11</p>	 <p style="text-align: center;">M18</p>

Table 2. LC-accurate mass measurements and in-source fragmentation of muraglitazar metabolites from human feces and microbial incubations

Metab. #	Formula and Mass ^a	Molecular Ions ^b		Major Fragment Ions ^c	
		Fecal	Microbial	Fecal	Microbial
M1	C ₁₇ H ₁₈ NO ₆ , 332.1134	ND	332.1143	ND ^d	226.0726
M2	C ₂₈ H ₂₇ N ₂ O ₈ , 519.1767	519.1790	519.1779	308.1304	308.1295, 202.0872
M3	C ₂₉ H ₂₉ N ₂ O ₉ , 549.1873	549.1937	549.1880	ND	324.1247
M4	C ₂₉ H ₂₉ N ₂ O ₉ , 549.1873	549.1899	549.1882	ND	324.1244, 306.1138
M5	C ₂₈ H ₂₇ N ₂ O ₈ , 519.1767	519.1747	519.1782	308.1273, 290.1187	308.1300, 290.1189
M6	C ₂₈ H ₂₇ N ₂ O ₈ , 519.1767	519.1799	519.1795	ND	308.1296, 202.0874
M7	C ₂₈ H ₂₇ N ₂ O ₈ , 519.1767	519.1774	519.1790	ND	290.1191, 202.0875
M8a	C ₂₉ H ₂₉ N ₂ O ₈ , 533.1924	533.1902	533.1984	308.1286	308.1308, 202.0884
M8	C ₂₉ H ₂₉ N ₂ O ₉ , 549.1873	549.1888	549.1877	ND	324.1244
M9	C ₂₇ H ₂₆ N ₂ O ₈ Na, 529.1587	529.1620	529.1611	282.1148, 176.0726	282.1140, 176.0723
M10	C ₂₉ H ₂₉ N ₂ O ₈ , 533.1924	533.1924	533.1951	308.1303, 290.1191	308.1303, 290.1195
M11	C ₂₉ H ₂₉ N ₂ O ₈ , 533.1924	533.1937	533.1960	308.1295	308.1307, 202.0884
M12	C ₂₉ H ₂₇ N ₂ O ₉ , 547.1717	547.1710	547.1742	322.1089	322.1093, 216.0669
M14	C ₂₉ H ₂₉ N ₂ O ₈ , 533.1924	533.1934	533.1946	290.1186, 202.0884	290.1192, 202.0880
M15	C ₂₈ H ₂₇ N ₂ O ₇ , 503.1818	503.1840	503.1835	292.1349	292.1347, 186.0929
M16	C ₂₉ H ₂₈ N ₂ O ₉ Na, 571.1693	571.1708	571.1714	324.1244	324.1249, 282.1136
Parent	C ₂₉ H ₂₉ N ₂ O ₇ , 517.1975	517.1993	517.1994	292.1342, 186.0927	292.1346, 186.0929

^a The molecular ions of M9 and M16 are [M+Na]⁺ ions, all others are [M+H]⁺ ions.

^b The lock mass used for the accurate mass measurement is 556.2771 Da.

^c The fragment ions listed here are from in-source fragmentation in Q-TOF analysis. More in-source fragmentation ions were detected in the microbial incubations because of higher concentrations of metabolites than those in human feces.

^d ND = Not Detected.

DMD 7153

Table 3. ^1H NMR assignments of muraglitazar metabolites

^1H #	Chemical Shifts (ppm)					
	M9	M10	M11	M14	M15	Parent ^a
2	3.95/4.01	3.84/3.89	3.85	3.88/3.93	3.81/3.84	3.92/3.98
3	4.52/4.65	4.46/4.58	4.49/4.63	4.51/4.64	4.49/4.57	4.47/4.60
5	6.97	6.90	6.92	6.97	7.00	6.91
6	7.31/7.33	7.25/7.29	7.26/7.29	7.29/7.32	7.28	7.25/7.27
8	4.37	4.27	4.27	4.27	4.47	4.23
9	3.27	3.02	2.93	5.04	3.00	2.92
12	-	4.60 ^b	2.35	2.47	2.29/2.31	2.35
15	7.92	8.00	7.80	7.99	7.91/7.96	7.94
16	7.56	7.50	6.92	7.53	7.55	7.48
17	7.67	7.50	-	7.52	7.57	7.47
20	6.94	6.90	6.93	6.97	6.96	6.89
21	7.04	7.00	7.04	7.04	7.04	7.00
23	3.81	3.77	3.81	3.81	-	3.77

The number system was shown in Figure 1. ND = not determined.

^a In D₂O/CD₃CN. ^1H NMR in D₂O/CD₃CN and in CDCl₃ were not significantly different. ^{13}C NMR (CDCl₃) in ppm: 173.19 (1), 47.39 (2), 51.28 (3), 128.48 (4), 114.83 (5), 130.18 (6), 158.57 (7), 66.77 (8), 26.06 (9), 132.42 (10), 145.38 (11), 10.31 (12), 159.80 (13), 127.29 (14), 126.16 (15), 128.82 (16), 129.29 (17), 155.54 (18), 114.91 (19), 130.18 (20), 122.62 (21), 144.86 (22), 55.67 (23).

^b Hydroxymethyl group

Figure 1

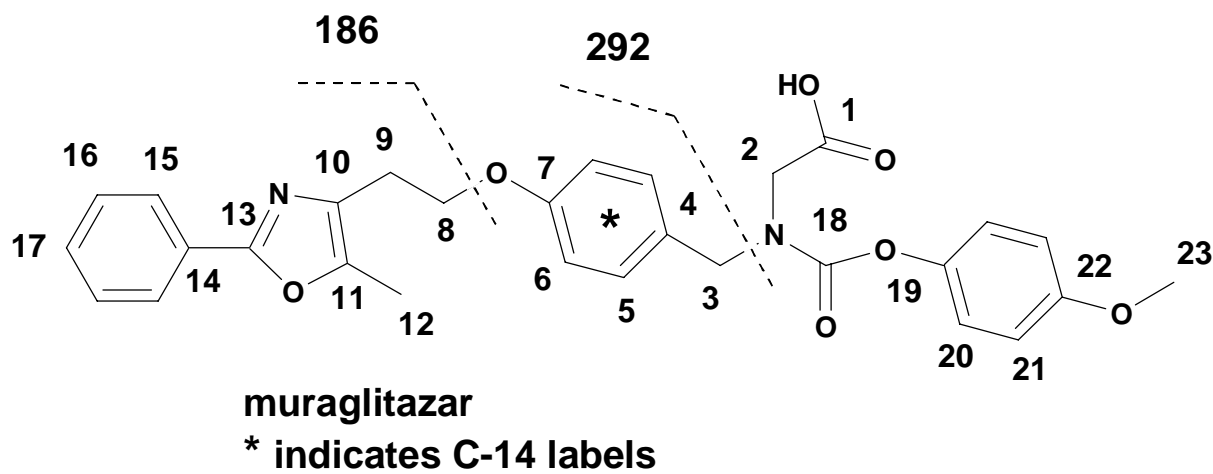


Figure 2

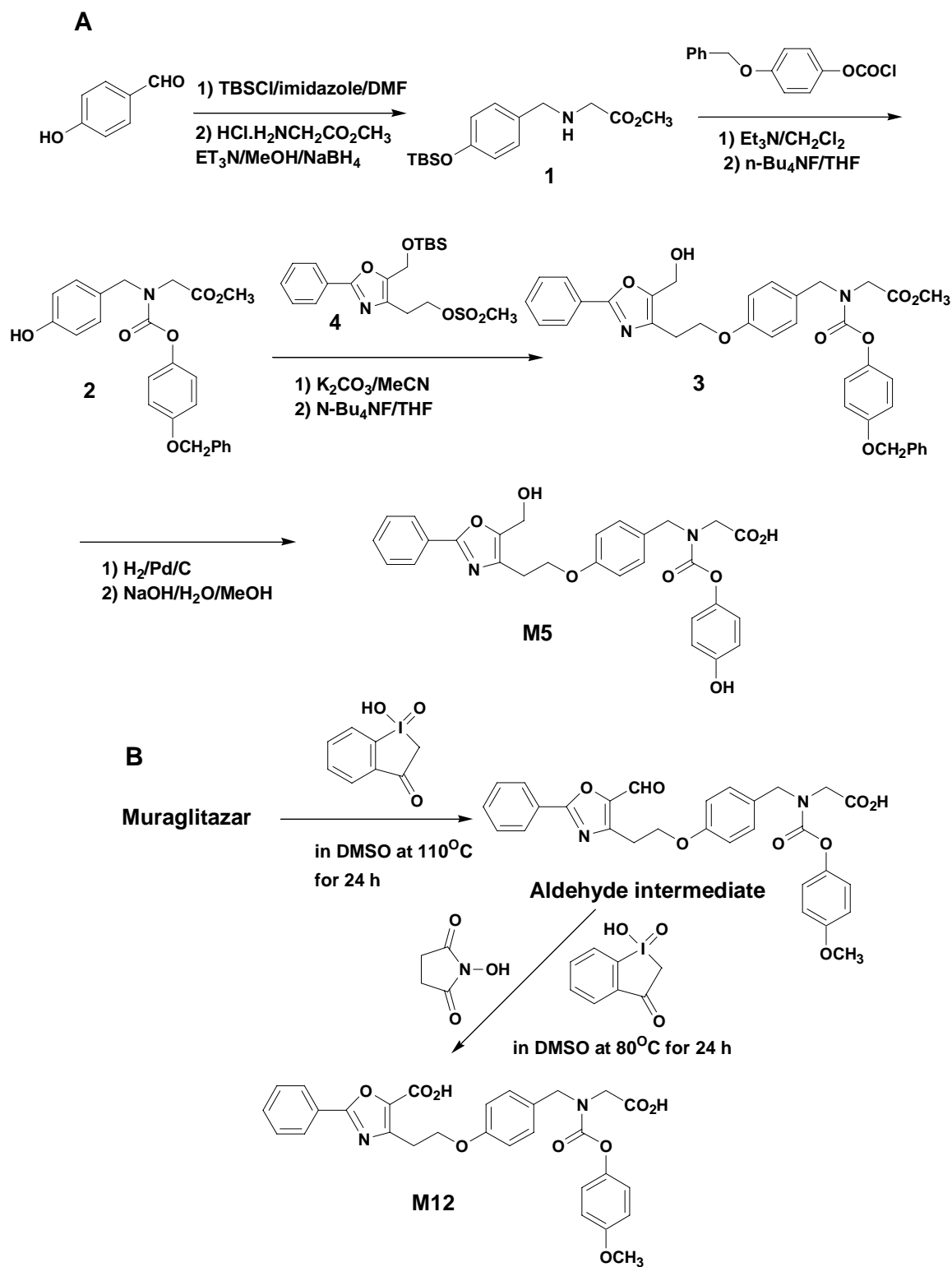


Figure 3

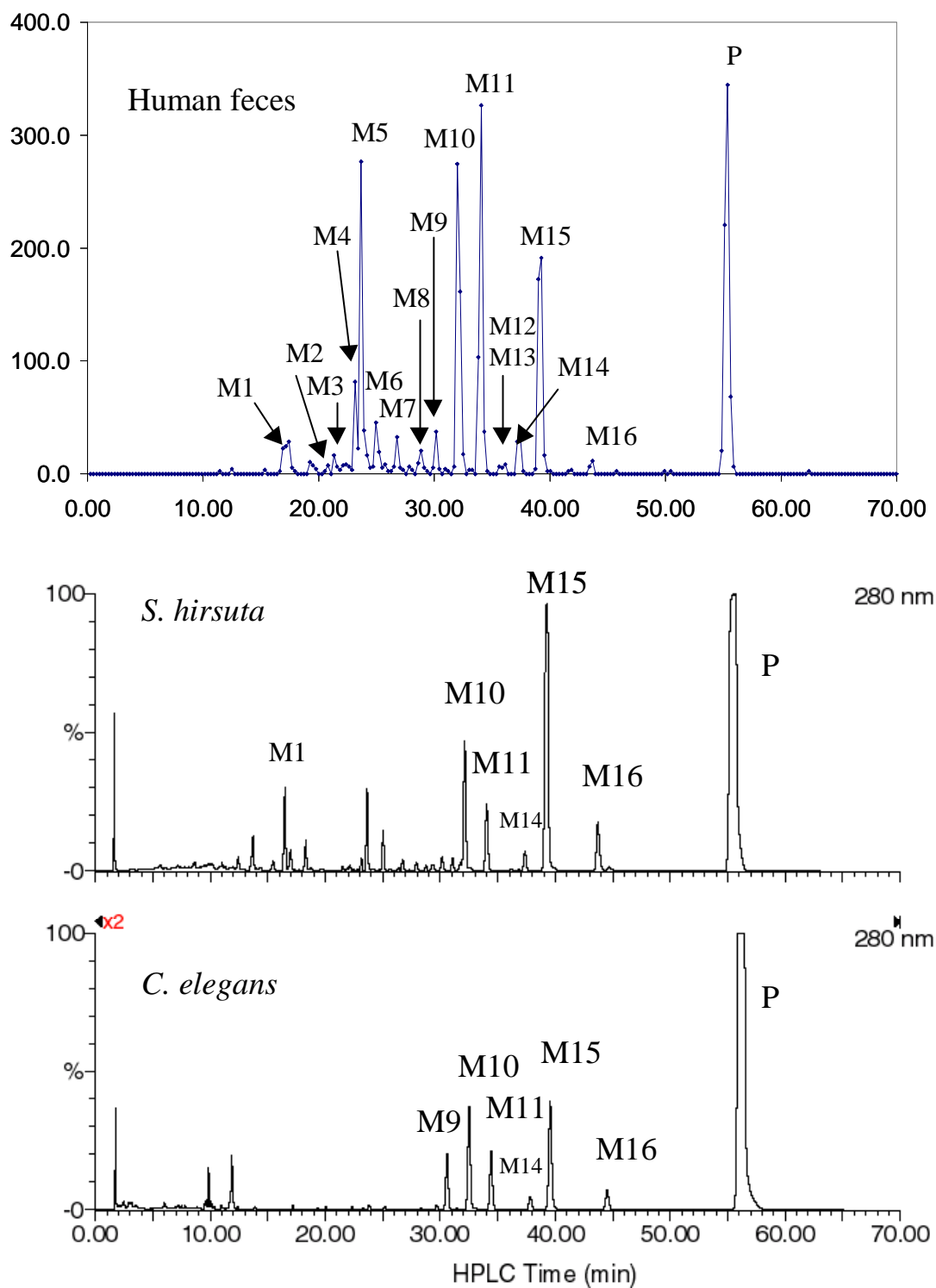


Figure 4

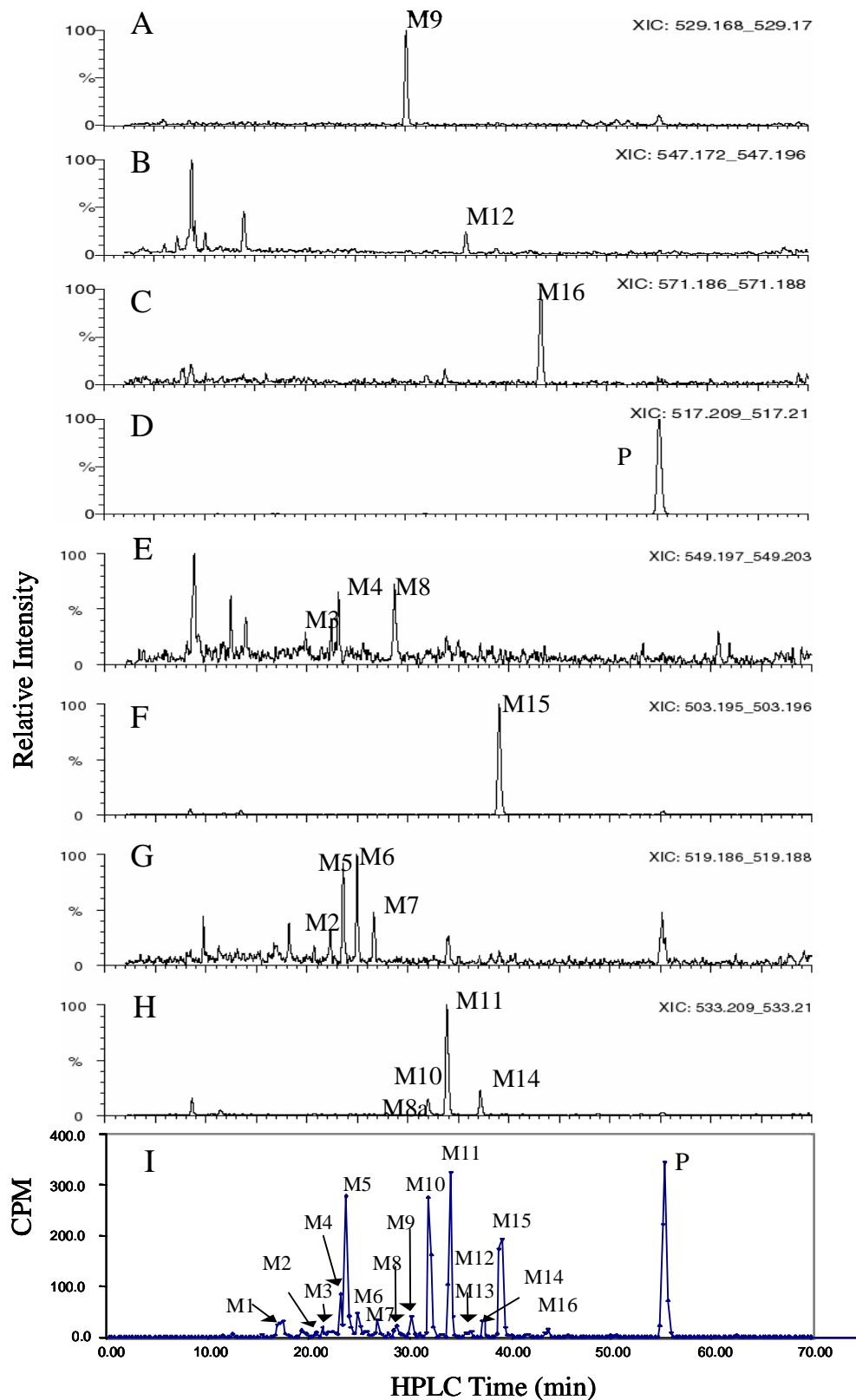


Figure 5

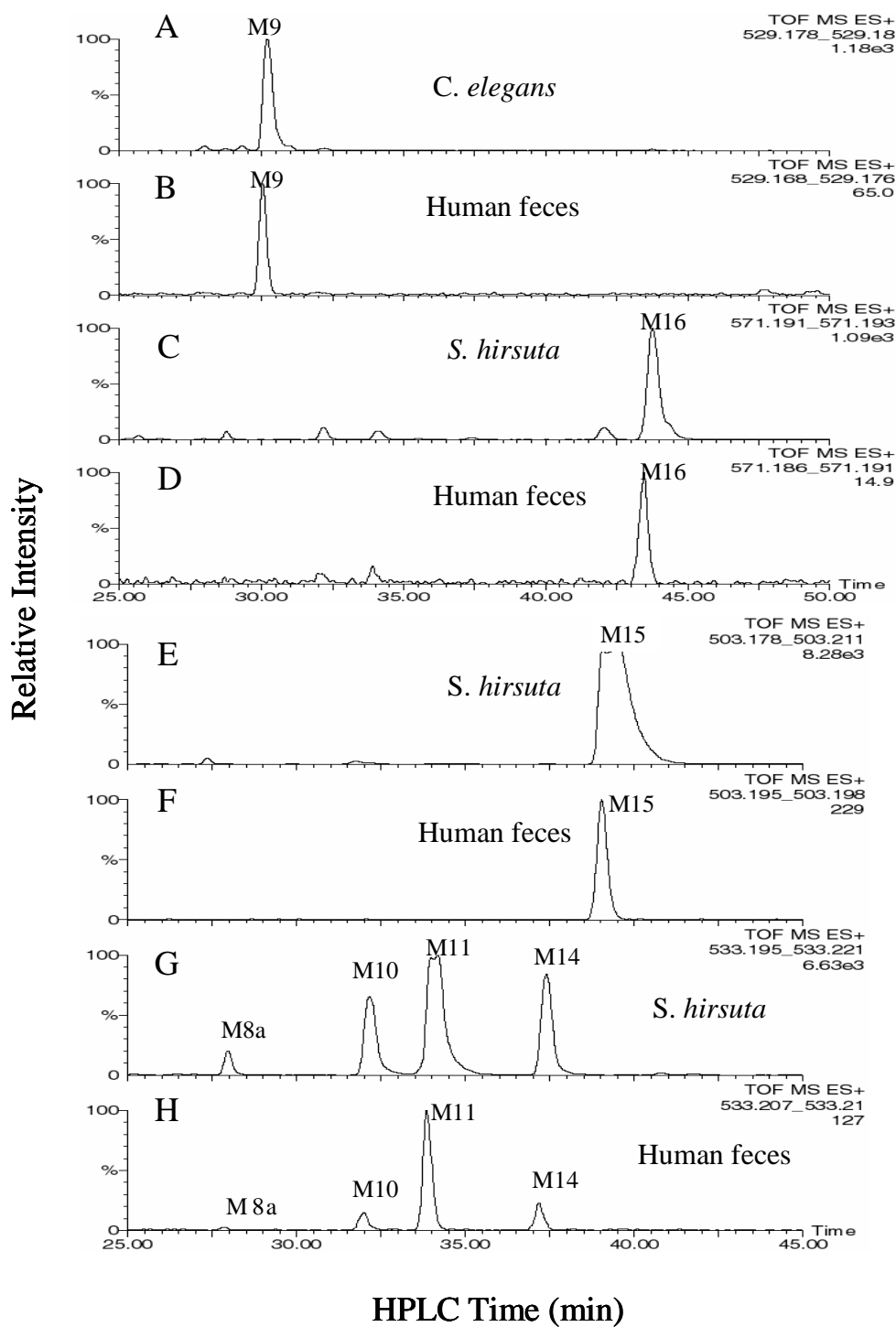


Figure 6A

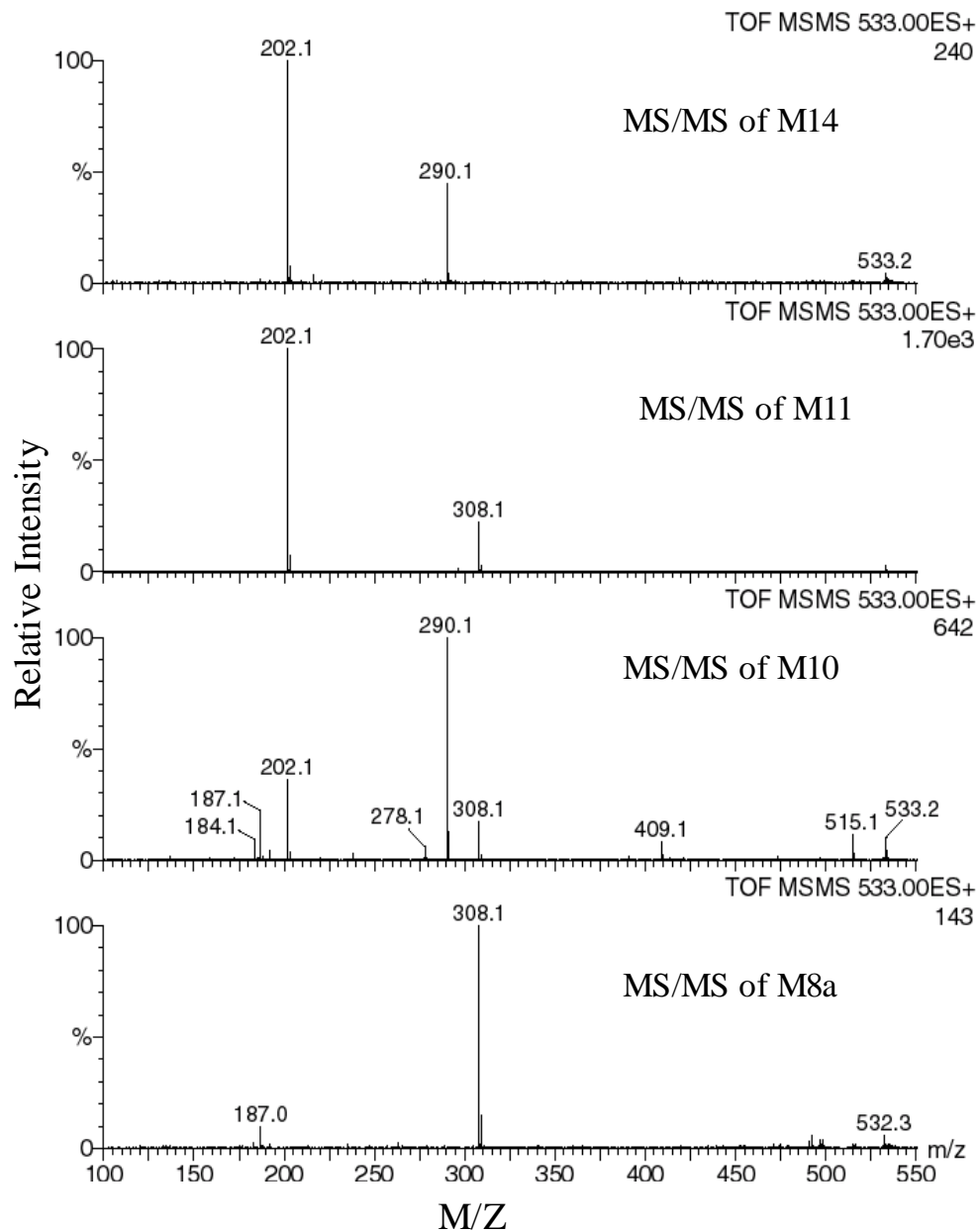


Figure 6B

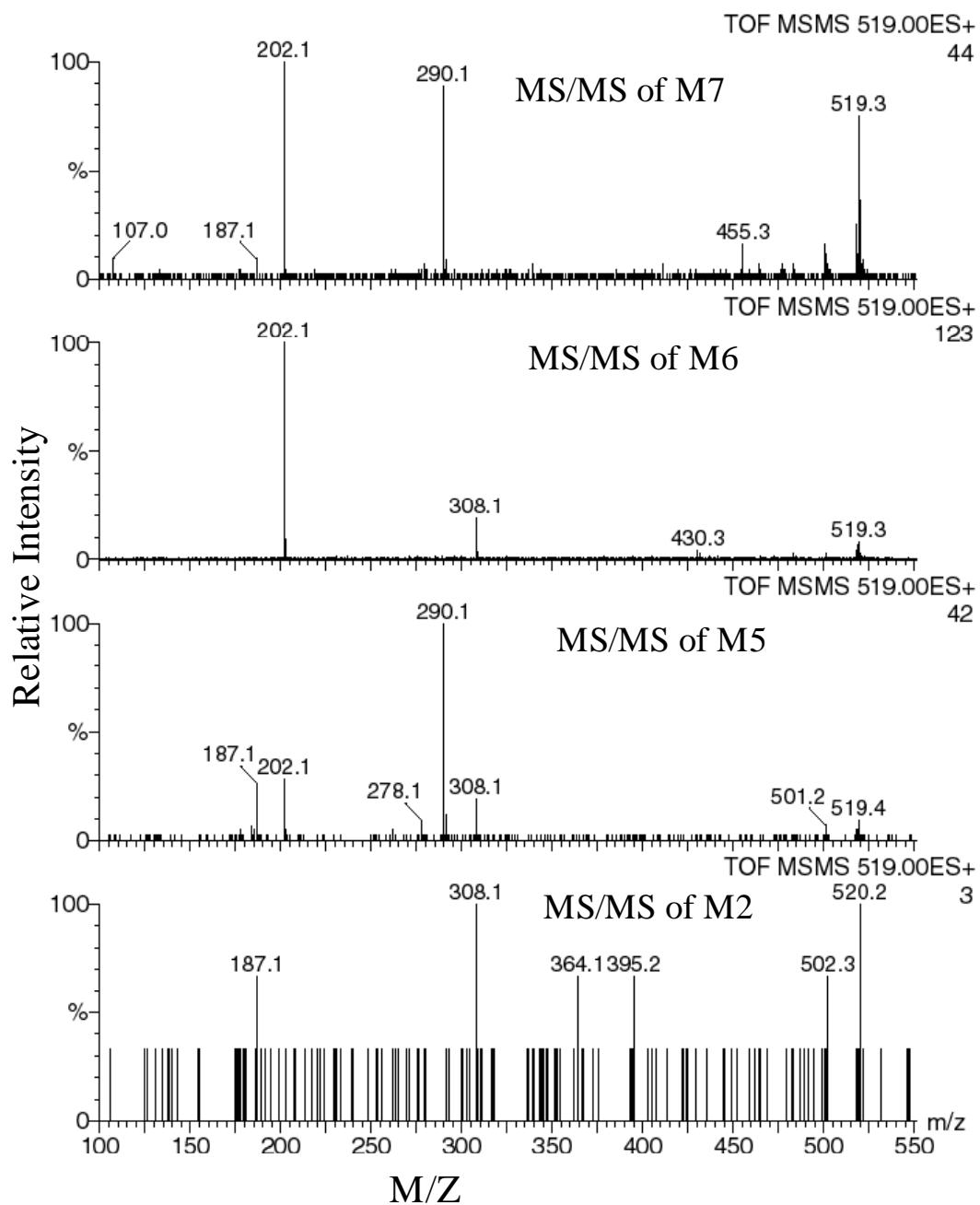


Figure 6C

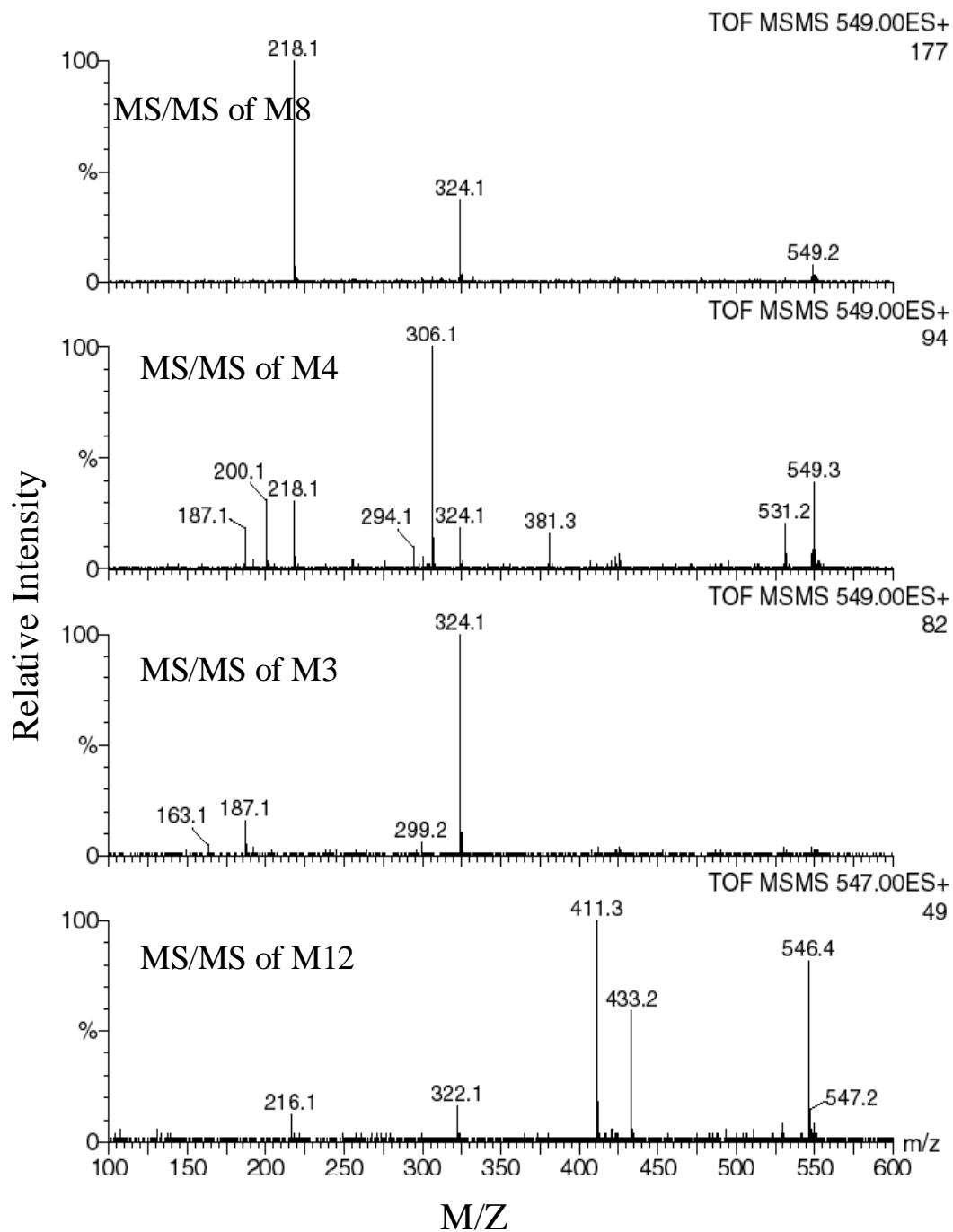


Figure 7A

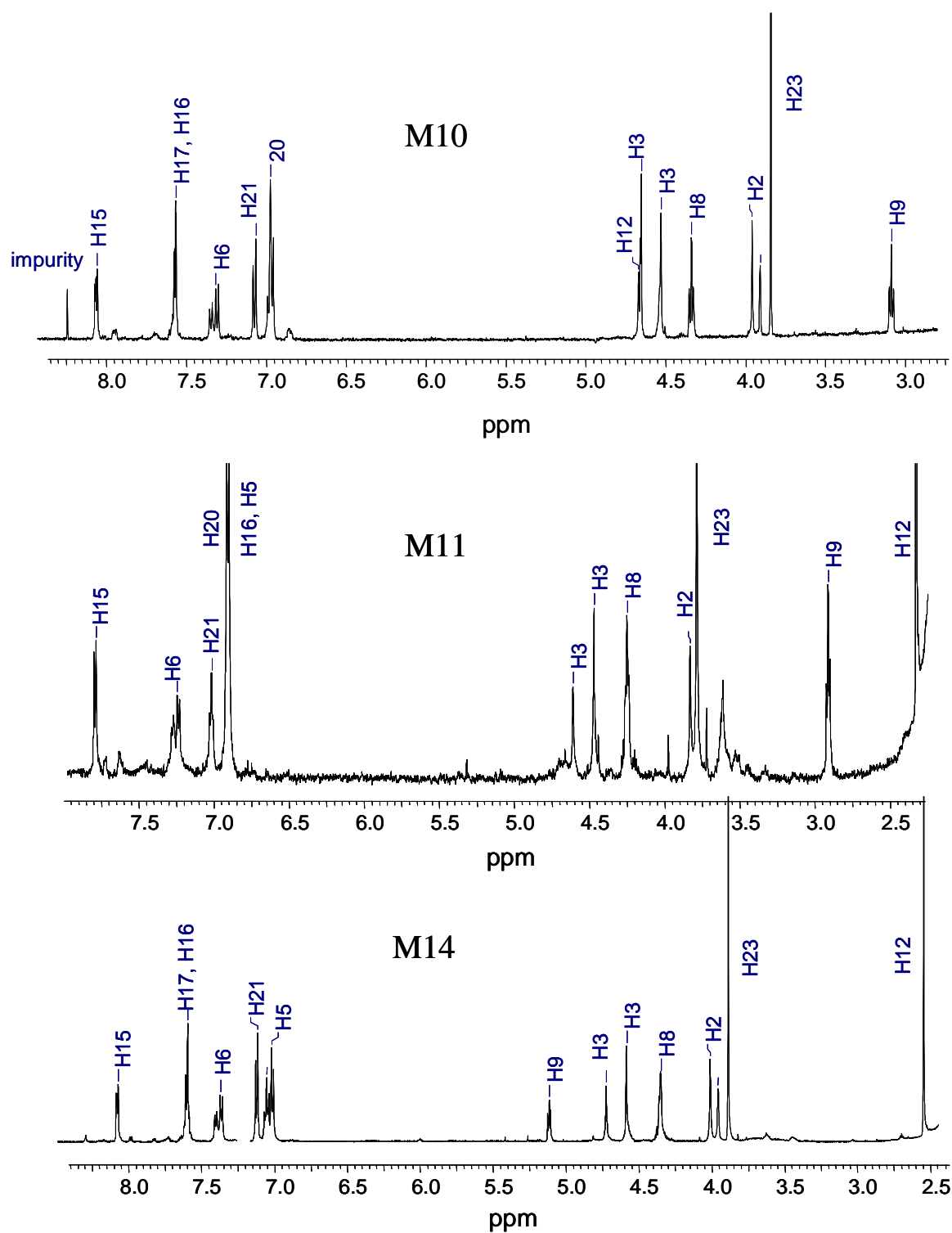


Figure 7B

